Available online at www.sciencedirect.com
SCIENCE DIRECT®
International Journal of Heat and Fluid Flow 24 (2003) 322–333
International Journal of HEAT AND FLUID FLOW
www.elsevier.com/locate/ijhff

Flow transition behind a heated cylinder

A.A. van Steenhoven, C.C.M. Rindt *

Department of Mechanical Engineering, Eindhoven University of Technology, WH-3.129, P.O. Box 513, 5600 MB Eindhoven, The Netherlands

Abstract

For more than a century the wake flow behind a cylinder has been the subject of many investigations. Most attention has been focussed on the first instability and the transition towards 3D for the flow around an unheated cylinder. The wake stability for a heated cylinder has until now received very little attention compared to the forced convection case. After a review of the literature on the wake flow behind an unheated and heated cylinder, in this paper the 2D wake behaviour and the 3D flow transition behind a heated cylinder are described. In the analysis performed, the Reynolds number is set around $Re_D = 100$ and the Richardson number is varied between $Ri_D = 0$ (forced convection case) and $Ri_D = 1.5$ (mixed convection case). From the results it is seen that for a relatively small heat input ($Ri_D < 1$) the vortex street undergoes *a negative deflection*, i.e. downwards, caused by a strength difference between the upper and lower vortices which, in turn, is induced by baroclinic vorticity production. This strength difference also results in *a rotational drift* of the lower vortex around the upper vortex. For a higher heat input ($Ri_D > 1$) *an early 3D transition* is observed. Mushroom-type structures appear on top of the upper vortex row. This flow transition is initiated by the occurrence of 3D flow structures at the rear end of the cylinder.

1. Literature review

The configuration studied in this paper consists of a horizontal heated cylinder with constant wall temperature T_1, which is exposed to a uniform horizontal cold cross-flow with velocity U_0 and temperature T_0. The cylinder has an outer diameter D and a length L, resulting in an aspect ratio $\mathscr{A}$ equal to L/D. The flow is determined by the fluid properties (expressed by the Pr number $Pr = \nu/\kappa$), the strength of the forced main flow (expressed by the Reynolds number $Re_D = U_0 D/\nu$) and the heat-induced buoyancy effects (expressed by the Grashof number $Gr_D = (T_1 - T_0)D^3 g\beta/\nu^2$). The relative importance of the forced and buoyant effects is indicated by the Richardson number ($Ri_D = Gr_D/Re_D^2$). In the definition of the above dimensionless numbers, κ denotes the thermal diffusity, ν the kinematic viscosity, g the gravity constant and β the thermal expansion coefficient.

1.1. Unheated cylinder

Over the last decade, a number of studies have focussed on the wake stability for an 'unheated' cylinder in the low Reynolds number range ($Re_D < 300$) (see e.g. Wu et al., 1996; Williamson, 1996; Zhang et al., 1995). For a forced-convection flow with Reynolds numbers between 50 and 190, the flow is 2D and behaves as fully periodic. This periodicity is created by the sequential shedding of vortex structures originating in the shear layers at both the upper and lower sides of the cylinder. These vortex structures form a street of 2D vortices consisting out of two vortex rows (Fig. 1:left): one row of clockwise rotating structures (negative vorticity) positioned above a row of counter-clockwise rotating structures (positive vorticity). The vortices in both rows form a staggered pattern, in which vortices in the upper row are shifted about half a streamwise vortex spacing with respect to the vortices in the lower row. For a forced-convection flow, this staggered pattern appears to be very stable and is most frequently referred to as the von Kármán vortex street. The alternate arrays of eddies were sketched by Bénard (1908). von Kármán and Rubach (1912) discovered that this vortex street could only be stable for a well-defined configuration ($a/b = 0.28056$, see Fig. 1:left). To that end, he introduced a

* Corresponding author. Tel.: +31-40-247-2978; fax: +31-40-243-3445.
E-mail address: c.c.m.rindt@tue.nl (C.C.M. Rindt).

0142-727X/03/$ - see front matter © 2003 Elsevier Science Inc. All rights reserved.
doi:10.1016/S0142-727X(03)00023-7

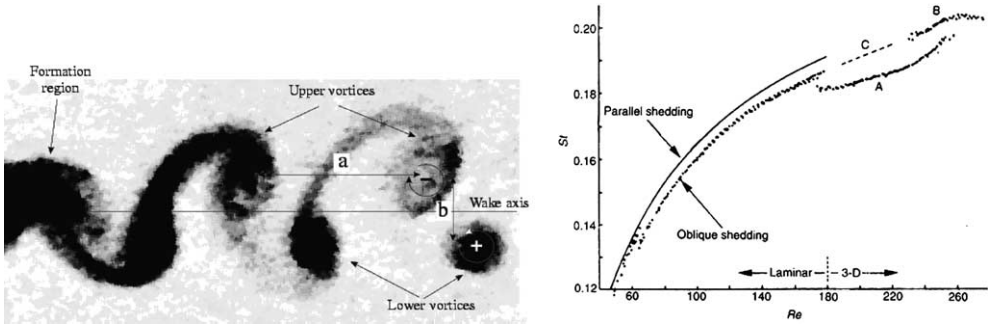

Fig. 1. Terminology for vortex shedding shown in a visualisation result for $Re_D = 73$ (left) (from Kieft et al., 2002a) and Strouhal–Reynolds number relationship over laminar and three-dimensional transition regimes (right) (from Williamson, 1996). Without a heat input 3D-transition takes place at $Re_D \approx 180$. A, B and C refer to different three-dimensional shedding modes.

point-vortex street in which he considered an eddy as a single point-vortex (von Kármán and Rubach, 1912).

The dynamics of the vortex street have drawn a lot of attention. Many researchers have investigated the forced-convection vortex street for a wide range of Reynolds numbers by means of visualisation experiments and hot-wire anemometry. For $Re_D < 4$ a creeping flow around the cylinder is observed in which viscous effects dominate. For this particular situation an analytical solution can be derived. A further increase of Re_D results in a flow in which a stable pair of vortices can be observed in the cylinder near wake. For $Re_D \approx 50$ this twin vortex configuration becomes very sensitive to disturbances, leading to a flow where vortices are shed sequentially at upper and lower sides of the cylinder. This sequential shedding of 2D vortex structures causes the wake flow to behave as fully periodic, with a natural frequency f. The non-dimensional representation of this frequency, the Strouhal number ($St = fD/U_0$), starts initially at $St \approx 0.11$ and then gradually increases as Re_D increases (Fig. 1:right).

By performing detailed particle tracking velocimetry (PTV) experiments, the vortex formation and shedding processes were investigated thoroughly (Green and Gerrard, 1993). It turned out that for $50 < Re_D < 100$ the vortex formation and shedding process is dominated by shear phenomena and that for higher Reynolds numbers inertia takes over. These observations suggest that the shedding mechanism is dependent on Re_D, especially in the regime where the shedding process is 2D. This can also be seen from the dependency of the Strouhal number on the Reynolds number. By increasing Re_D, viscous effects become less important. This decrease of viscous effects then causes the vortex shedding mechanism to depend more on convection, resulting in an almost constant St number. This appears to happen for $Re_D \approx 500$.

The measurements for small Re_D show some irregularities around $Re_D = 60$ and 100. It turns out that these irregularities are due to oblique vortex shedding, which implies that the vortex tubes are slanted with respect to the cylinder axis. This oblique shedding is caused by the end effects of the cylinder (Slaouti and Gerrard, 1980). For a very large cylinder aspect ratio, $\mathscr{A} > 150$, oblique shedding almost does not occur in the interior region. By installing proper cylinder ends, as for example end plates or diameter thickening, the oblique shedding can be suppressed (Williamson, 1989). By increasing Re_D above 200, 3D modes arise in the cylinder wake (Eisenlohr and Eckelmann, 1989; Karniadakis and Triantafyllou, 1992).

Over the last 10 years, a lot of attention has been paid to the three-dimensional vortex dynamics behind a cylinder. Experimental and theoretical studies of 3D wake transition have made a lot of progress (Williamson, 1996; Barkley and Henderson, 1996). Direct numerical simulations (Mittal and Balachandar, 1996) have contributed significantly to the understanding of 3D wake flows. The transition to three-dimensionality in the wake can be conveniently illustrated using a relationship of the Strouhal–Reynolds number (Fig. 1:right).

The 3D wake transition is originally described by Roshko (1954), based on the measurement of velocity spectra. A visualisation of the flow by Hama (1957) showed that the instability in the wake transition region takes the form of a three-dimensional waviness of the von Kármán vortices. It is essentially what Gerrard (1978) later called "finger of dye". Williamson's flow visualisations (1988, 1992) showed that Gerrard's dye fingers are associated with vortex loops and streamwise vortices. He suggested two different modes, mode-A and mode-B instability, scaling on different physical features of the flow.

First the primary vortices deform in a wavy fashion along their length during the shedding process. This results in the local spanwise formation of vortex loops, which become stretched into streamwise vortex pairs. The spanwise lengthscale of these structures is typically 4 cylinder diameters. This is known as the A-mode of instability. For slightly higher Reynolds numbers a gradual transfer of energy takes place from the A-mode to a B-mode of instability, which is characterized by

finer-scale streamwise vortex pairs with a spanwise lengthscale of typically 1 cylinder diameter.

The two modes of instability scale on two principal physical features of the wake flow; the primary vortex cores (mode-A) and the braid shear layer (mode-B). The formation of vortex loops in the A-mode of instability appears to be coupled to a spanwise waviness in the primary vortex cores. The streamwise vortices occurring for the B-mode of instability originate from a spanwise waviness in the braid shear layer. The appearance and formation of these streamwise vortices for both mode A and mode B are highly determined by the vorticity distribution, streamline pattern (the occurrence of a saddle point) and reversed flow region in the vicinity of the cylinder (Williamson, 1996).

The process of transition is complicated by the existence of vortex dislocations, triggered at the sites of the vortex loops of mode-A instability. These dislocations are responsible for the stable and unstable states of the wake through the transition regime (Williamson, 1992).

1.2. Heated cylinder

Despite the fact that mixed convection around bluff bodies is of great importance for various engineering applications (electronics cooling, compact heat exchangers) wake stability for a heated cylinder has until now received very little attention compared to the forced convection case.

The effect of heat on the cylinder wake is investigated less thoroughly. In the early seventies, this effect was investigated to determine the global effects of the induced heat on the heat exchange coefficient (Hatton et al., 1970). It turned out that for a value of the Richardson number larger than 0.2 the heat transfer coefficient was influenced considerably by the thermally induced flow. These investigations were carried out for various angles between the gravity vector and the main flow direction, and resulted in a set of critical Ri_D values above which thermal effects influence the heat exchange coefficient. In the investigations the circumstances could be established under which hot-wire velocity measurements could be applied, but almost no attention was paid to the effect of heat on the wake structures and wake behaviour.

More detailed studies on the effect of heat on the vortex wake were carried out slightly later (Noto et al., 1985; Noto and Matsumoto, 1987; Badr, 1984) and some remarkable results were obtained. These studies describe the flow around a heated horizontal cylinder exposed to a vertically upward directed flow. By increasing the heat input (increasing Ri_D), the Strouhal number first increases. However, above a critical Richardson number, the Strouhal number becomes zero and vortex shedding is suppressed. For this heat input the vortex street converts again to a wake in which two twin vortices are situated in the near wake. A further increase of the heat input causes these vortices to disappear, ending up with a thermal plume. The influence of buoyancy on the vortex shedding frequency was further analysed numerically by Chang and Sa (1990) and Singh et al. (1988). The same results were obtained in experiments performed by Michaux-Leblond and Bélorgey (1997) and here the dualism between buoyancy and viscous effects was considered to be the source of the sudden disappearance of the vortex shedding phenomenon.

Even more interesting for this paper is the situation where the heated cylinder is exposed to a non-vertical cross-flow. The non-parallelism between the cross-flow direction and the buoyant force causes the flow pattern to become asymmetric, with the vortices in the upper vortex row having slightly different characteristics compared to the vortices in the lower row. The effect of the angle between the main flow direction and the gravitational vector was numerically investigated by Noto (1991). From this study it was found that the angle of attack has a major influence on the vortex street characteristics. Starting with an angle of 180° (corresponding to a vertical upward flow) it was found that first the vortex shedding was suppressed by an increasing heat addition. When the angle of attack was decreased, the wake became periodic again, while for angles smaller than 90°, the natural frequency was found to become even larger than for the unheated situation. Also for the horizontal flow situation it was observed that for Reynolds values just above the critical value ($Re_c = 49$) the vortex shedding could be suppressed by heating of the cylinder (Lecordier et al., 1991; Wang et al., 2000). In Lecordier et al. (2000), the sudden disappearance of the vortex shedding phenomenon is analysed and it is concluded that the influence of the temperature on the viscosity is the primary source. In fact, an increase of the temperature leads to a decrease of the effective Reynolds number. In Mi and Antonia (1994) the temperature distribution within vortices in the wake of a cylinder is studied and they concluded that this distribution is quite well approximated by the theoretical distribution for a diffusing line vortex.

The effect of a heat input on the behaviour of coherent structures shed from a cylinder will be the main subject of this paper. Revealing the processes and mechanisms involved in the heat-induced change of the structure characteristics and early wake transition will be the main focus. These processes are studied for flows which are initially two-dimensional and for which the shedding mechanism is constant ($Re_D \approx 75$). Therefore the influence of the heat input is fully expressed in the variation of Ri_D ($0 < Ri_D < 2$). In this paper previous research is reviewed and some new data is added.

The investigation of this problem is performed both numerically and experimentally. First the problem

definition will be given together with the describing equations. The experiments were performed in a towing tank, in which the flow characteristics were measured by using high resolution particle velocimetry (HiRes-PV). Hence, both the experimental set-up and the applied HiRes-PV technique are described. For the numerical study a spectral element method was employed, allowing to calculate the flow field with a high accuracy. Also a brief introduction is given to this method. Finally, the effect of a heat input on the wake characteristics and the behaviour of the vortex structures further downstream will be presented as well as a detailed description of the effect of heat on the vortex shedding process. At the end, some conclusions are formulated.

2. Heated cylinder flow problem

As mentioned before the problem under consideration (Fig. 2) consists of a horizontal cylinder heated to a constant temperature and placed in a uniform horizontal cross-flow. The flow is described in terms of a Cartesian x, y, z-coordinate system, with x pointing in the (horizontal) direction of the main flow, z pointing in the spanwise direction, while the y-direction is vertically upwards (antiparallel with the gravitational acceleration).

For small temperature differences the Boussinesq approach can be applied. By scaling the velocities by U_0, the spatial coordinates by D, the time by D/U_0, the pressure by ρU_0^2, the temperature by ΔT (with $\Delta T = T_1 - T_0$) and the gravitational acceleration by its magnitude g, the flow can be described by the dimensionless conservation equations for mass, momentum and heat:

$$\nabla \cdot \vec{u} = 0, \tag{1}$$

$$\frac{\partial \vec{u}}{\partial t} + \vec{u} \cdot \nabla \vec{u} = -\nabla p + \frac{1}{Re_D} \nabla^2 \vec{u} - Ri_D \Theta \vec{g}, \tag{2}$$

$$\frac{\partial \Theta}{\partial t} + \vec{u} \cdot \nabla \Theta = \frac{1}{Re_D Pr} \nabla^2 \Theta, \tag{3}$$

with $\vec{u}$, Θ, p and $\vec{g}$ the dimensionless velocity vector, the temperature, the pressure and the gravitational vector, respectively. The Reynolds number in this paper is around a value of 100. The Richardson number, expressing the relative importance of the buoyancy term in the momentum equation, is varied from 0 to 1.5, which corresponds to temperature differences for water in the range of $0 < \Delta T < 7$ °C.

Assuming a 2D flow in the x, y-plane, the vorticity vector $\vec{\omega}$ is directed in the z-direction, i.e. $\vec{\omega} = (0, 0, \omega_z)$. The vorticity equation (derived by taking the curl of the momentum equation) then reduces to a scalar transport equation, written as

$$\frac{\partial \omega_z}{\partial t} + \vec{u} \cdot \nabla \omega_z = \frac{1}{Re_D} \nabla^2 \omega_z + Ri_D \frac{\partial \Theta}{\partial x}, \tag{4}$$

with ω_z the out-of-plane component of the vorticity vector $\vec{\omega}$, defined as

$$\omega_z = \frac{\partial v}{\partial x} - \frac{\partial u}{\partial y}. \tag{5}$$

The second term on the right-hand side of (4) is the so-called baroclinic production term, representing production of vorticity within the flow domain due to temperature gradients perpendicular to $\vec{g}$.

In Fig. 3:top the results of a hydrogen bubble visualisation of the wake behind a heated cylinder for $Ri_D = 0.5$ and $Re_D = 75$ is shown. The remarkable

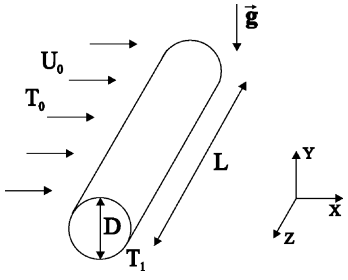

Fig. 2. Problem definition.

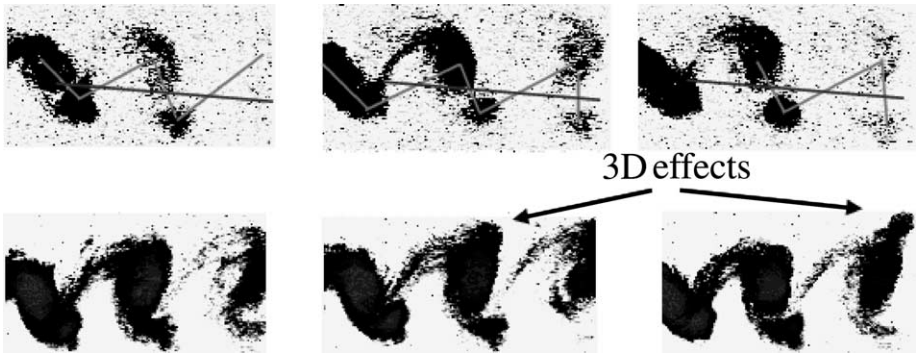

Fig. 3. Hydrogen bubble visualisations: side-view. $Re_D = 75$ and $Ri_D = 0.5$ (top) and $Ri_D = 1.5$ (bottom) (from Kieft et al., 2000b). The solid lines in the top-figure indicate the wake axis and the staggered pattern of the vortex centres.

downward deflection of the vortex street is caused by a strength difference between the upper and lower vortices. Besides this negative deflection, the strength difference also leads to a relative motion of two subsequently shed structures. The reason for the strength difference between the upper and lower vortex row lies in the baroclinic vorticity production induced by the heat input. In Fig. 3:bottom results of a hydrogen bubble visualisation are shown at a higher Richardson number, $Ri_D = 1.5$. An early transition towards 3D is found, which manifests itself as the occurrence of mushroom-type structures on top of the upper vortex row. More details about the vortex street behaviour for lower heat inputs ($Ri_D < 1$) and the 3D transition for higher heat inputs ($Ri_D > 1$) will be given below.

3. Experiments and numerics

3.1. Experimental set-up

A towing tank apparatus has been designed which allows to perform detailed experiments on the flow behind the cylinder. The cylinder is towed through the water tank (Fig. 4). The cylinder, with diameter $D = 8.5 \times 10^{-3}$ m and length $L = 0.495$ m, is kept in position by two perspex plates (Fig. 4:right) with dimensions width $\times$ height $= 0.50$ m $\times$ 0.65 m (thickness 4×10^{-3} m). The plates are connected to a stiff structure, carrying the cylinder and the measuring equipment. The carrier can translate at a prescribed constant speed U_0 (up to 0.03 m/s) along two guiding rails with a variation of less than 0.2%.

The specific dimensions of the towing tank are length $\times$ width $\times$ height $= 5$ m $\times 0.50$ m $\times 0.75$ m (Fig. 4:left). For $Re_D \approx 100$, the length of the tank allows to measure about 40 characteristic shedding periods of the specific flow problem. The width of the tank is chosen such that the relative thickness of the boundary layers along the carrying plates (Fig. 4:right) is small. Any direct influence of the boundary layer on the vortex shedding in the cylinder wake halfway along the span of the tank can therefore be neglected. An indirect influence, such as oblique vortex shedding may still be present (Williamson, 1989). However, this oblique shedding turns out to be suppressed by the end plates between which the cylinder is clamped. More information about the measuring device, its accuracy, and the measurement procedure can be found in Kieft et al. (1999b).

3.2. Measuring techniques

For the 2D velocity experiments a hybrid measurement technique between particle tracking velocimetry (PTV) and particle image velocimetry (PIV) is used, a so-called high resolution particle velocimetry method (HiRes-PV). With this method about 7000–10,000 independent velocity vectors can be determined using a 1 k $\times$ 1 k camera. A detailed description of the relevant algorithm parts and a test on the performance of the algorithm on real fluid flow data is presented in Bastiaans et al. (2001).

Also preliminary 3D particle tracking experiments are carried out. The 3D-PTV method employed makes use of three cameras and the crossing-line method for localization of the particles. In the experiments about 500 vectors could be constructed, which is rather low compared to the 2D HiRes-PV method. Nevertheless, the 3D-PTV results resembled very well the results obtained with visualisation experiments (Kieft et al., 2002a,b).

Besides the above mentioned quantitative techniques flow visualisation experiments are also carried out using an electro-chemical method, in which a thin tin plate is positioned about 15D upstream of the cylinder. Dependent on the vertical position of the tin-plate the upper or lower vortex rolls are visualised. More information on the visualisation method can be found in Maas et al. (in press).

Laser induced fluorescence (LIF) is used to measure the instantaneous 2D temperature distribution in the

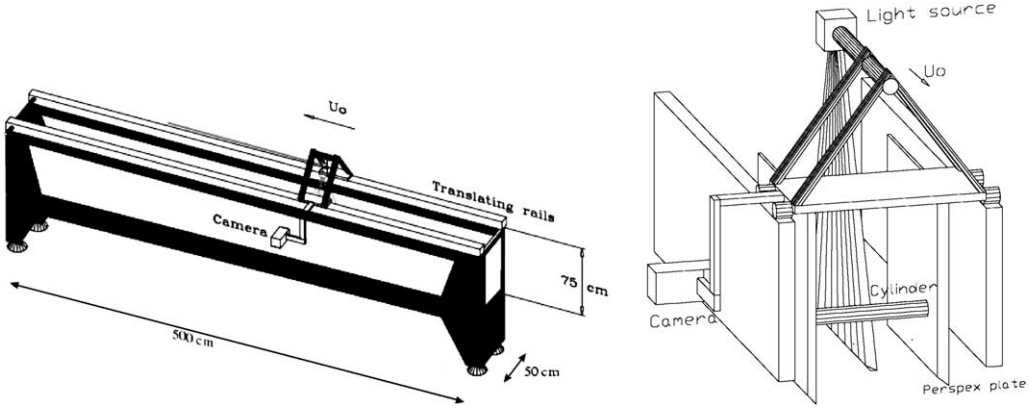

Fig. 4. The towing tank apparatus (left) and the carrier system (right).

wake of the heated cylinder. Rhodamine B, a fluorescent dye, is used as temperature indicator. The relation between fluorescence intensity and temperature is determined by means of calibration experiments in the temperature range of 20–35 °C with an accuracy of ±0.1 °C. More information on the method can be found in Coolen et al. (1999) and Seuntiëns et al. (2001).

3.3. Numerical method

Parallel to the experiments, 2D numerical simulations are performed. For an efficient temporal discretisation of the Boussinesq equations (1)–(3), the (non-)linear convection-diffusion equations are split (Minev et al., 1995). The convection equation is temporally discretised by applying a three-steps explicit Taylor-Galerkin scheme. The diffusion equation is discretised by an implicit second-order backward difference scheme. The pressure term arising in the diffusion equation as a kind of source term, is treated by an approximate projection scheme (Timmermans et al., 1996).

For the spatial discretisation a high-order spectral element method (SEM) is used which can be considered as a mixture of a finite element method (Cuvelier et al., 1986) and a spectral method. Here a ninth order approximation polynomial is used. A detailed study on the influence of the domain height (Kieft, 2000) has revealed that for values larger than 24D almost no influence of the upper and lower walls is observed. The length of the domain has no significant influence as long as the inflow wall is more than 8D upstream and the outflow wall more than 25D downstream of the cylinder. Though, the specific dimensions of the calculation domain chosen are length × height = 33 D × 24 D.

3.4. Data processing

In principle, the measured velocity field is an unstructured field. To calculate derived quantities such as vorticity, the unstructured field is transformed onto a structured grid (Agui and Jimenez, 1987). The vorticity component ω_z is calculated from the interpolated data on the structured grid by using a first-order central difference scheme. From the 2D vorticity field, some properties of the vortex structures can be derived. For the position of the structure, the vorticity centroid is used, its coordinates being defined by

$$X = \frac{1}{\Gamma}\int_A \omega_z(x,y)x\,\mathrm{d}A, \quad Y = \frac{1}{\Gamma}\int_A \omega_z(x,y)y\,\mathrm{d}A \tag{6}$$

with $\Gamma = \int_A \omega_z(x,y)\,\mathrm{d}A$ and A the area enclosed by the iso-vorticity contour $C(\omega_a)$. Here the closed iso-vorticity contour ω_a was set to $|\omega_a| = 0.2\,\omega_0$, with ω_0 being equal to U_0/D. This value of ω_a corresponds to about 10% of the maximum vorticity value just after the formation of the vortex structures.

4. 2D wake behaviour

4.1. Vortex dynamics

Starting from the experimental results, the behaviour of the vortex structures shed in the cylinder wake was analysed for several shedding periods. The interrogation window of these experiments was fixed with respect to the cylinder and occupies the area between $x = 0$ (the cylinder position) and $x = 25$. Note that the x- and y-positions are scaled with the diameter D. For a duration of 120 s (typical shedding period is 6 s), the vortex positions were calculated from the measured velocity field with intervals of 1 s. Results are shown in Fig. 5 for $Ri_D = 1$. This figure shows the trajectories of about 40 shed vortex structures. For both the upper and lower rows an exponential function, representing the average trajectory, is fit through the vortex positions (middle-figure). In the left-figure the vorticity contours, derived from the measured velocity field, are shown.

For $Ri_D = 0$ (results not shown here), the shed vortices form a regular von Kármán vortex street. The average trajectories for the upper and lower vortices show an almost symmetric profile with respect to the wake axis ($y = 0$). For increasing downstream position, both trajectories are deflected equally from the wake axis.

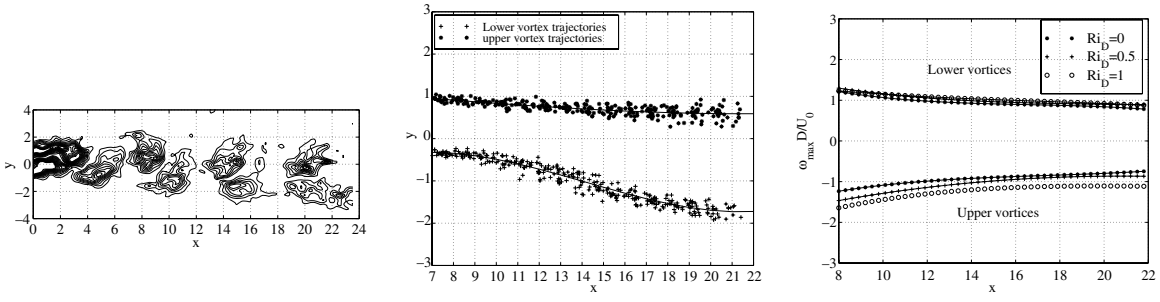

Fig. 5. Experimental HiRes-PV results for $Re_D = 75$, showing vorticity contours (left) and structure trajectories (middle) for $Ri_D = 1.0$ and the peak vorticity for various Ri_D values (right) (from Kieft, 2000). Note that the spatial coordinates are scaled with the diameter of the cylinder.

This deflection can be seen as a widening of the vortex street due to viscous spreading of the vortex cores (Green and Gerrard, 1991). For $Ri_D > 0$ an additional deflection of the vortex trajectories in negative y-direction is found. Keeping in mind the effect of buoyancy, one would intuitively expect the opposite, i.e. an upward deflection. This additional negative deflection is found to be larger for $Ri_D = 0.5$ than for $Ri_D = 1$. Besides, the deflection of the lower vortex row is larger than the deflection of the upper vortex row for $Ri_D = 0.5$.

Also interesting is the decreasing distance in x-direction between a subsequently shed lower and upper vortex. For increasing Ri_D the lower vortex moves more into the direction of the upper one. In combination with the observed relative motion in y-direction, it appears as if the lower vortex is slowly rotating underneath the upper vortex. This effect is clearly visible in Fig. 5:left and can also be noticed in the hydrogen bubble visualisation results (Fig. 3:top). More numerical and experimental results on this rotational drift can be found in Kieft et al. (in press). This rotational drift hints at strength differences between the vortices in the upper and lower rows.

As a measure of the strength of a vortex structure its peak vorticity value is used. The spatio-temporal evolution of the 'measured' strengths of the wake vortices is shown in Fig. 5:right for $Ri_D = 0$, 0.5 and 1. For increasing Ri_D, the extremes of the negative upper vortices increase (in absolute sense). In contrast, the lower vortex extremes do not show a strong dependence on Ri_D, implying an asymmetry in the wake. This asymmetry is already present just after the formation of the structures at $x = 8$. By using a point-vortex model it can be shown that the strength difference is indeed responsible for the observed negative deflection and rotational drift (Kieft et al., 1998, 1999a).

4.2. Baroclinic vorticity production

Within the near-wake ($x < 6$) several processes may lead to a difference in strength between the vortices. Considering the local increase of vorticity two contributions can be distinguished: diffusion of vorticity from the cylinder wall to the interior of the flow and thermally induced baroclinic vorticity production, represented by the first and the second term in the right-hand side of (4), respectively. An analysis of these terms in the vicinity of the cylinder ($x < 1$) reveals that the addition of heat results in more positive than negative vorticity entering the region $x > 1$. Therefore, it can be concluded that the earlier observed difference in strength between the upper and lower vortex structures can not be caused by vorticity sources in the vicinity of the cylinder.

The structure formation is also analysed in the downstream region $1 < x < 6$. Fig. 6 represents a snapshot of the spatial distribution of vorticity (left) and the baroclinic-vorticity production (right). From the vorticity production graphs it can be seen that when an upper vortex is initiated at $x \approx 1.7$, $y \approx 0.5$, an area of negative baroclinic vorticity production is located at the tip of the (negative) vorticity strand at $x \approx 1.7$, $y \approx 0.5$. The production term contributes therefore to the vortex structure to be formed. Slightly upstream at $x \approx 1$, $y \approx 0.5$, a small area of positive production can be found. This area coincides with the area where somewhat later the constriction of the vorticity strand takes place. It appears that in the first half of the formation period the production term adds to the newly formed negative upper structure. In the second half, the area of positive vorticity production just upstream of the negative production becomes almost as strong as the negative production. It is then expected that the absolute strength of the formed vortex structure is not much influenced anymore by these production terms.

During the formation of a lower vortex, again an area of negative and positive vorticity production is located in the region where the new vortex structure is formed. Especially in the early stage of the vortex formation process (between $1 < x < 3$) the production of negative vorticity is stronger. Therefore, in the first half of the formation process, a net amount of negative vorticity is produced within the lower vortex. This production causes the lower vortex to become weaker with respect to the situation for $Ri_D = 0$. In the second half of the

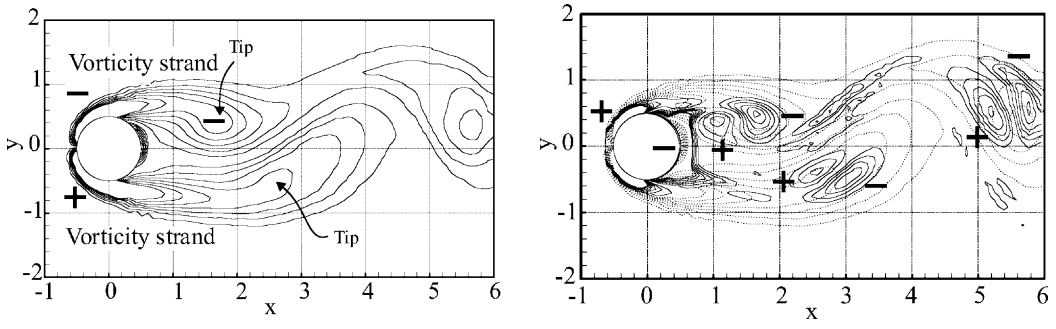

Fig. 6. Numerically calculated near-wake vorticity (left) and vorticity production (right) for $Re_D = 75$ and $Ri_D = 0.5$ at a distinct time level (from Kieft, 2000). The vorticity production graphs are drawn together with the vorticity distribution (dashed lines).

vortex formation process, the production of positive vorticity within the newly formed structure increases and becomes more or less equal to the contribution of the negative production, resulting in no net change of vortex strength.

5. 3D wake transition

5.1. Far-wake behaviour

Fig. 7 shows visualisation results of the wake flow for $Re_D = 116$ and $Ri_D = 1$ using a vertical laser-sheet positioned halfway along the width of the tank. Clearly visible in the left-figure are the mushroom-type structures on top of the upper vortex row. These structures start to develop at the third upper vortex and stretch in vertical direction when convected downstream. They look quite similar as the structures observed by Humphrey and Marcus (1987) in an unstably stratified flow with shear superimposed. That the structures found are really 3D can be concluded from the right-figure where a snap-shot of the wake flow is presented at a different moment in time. In the time-span between both figures the position for the occurrence of the mushroom-type structures has shifted in spanwise direction. In the right-figure they are still vaguely visible. In this 'between-plume' visualisation the wake flow manifests itself more or less as the regular von Kármán vortex street. Main difference with the von Kármán vortex street is the rotation of the lower vortex underneath the upper one. This rotation is also found in the 'in-plume' visualisation and, as discussed above, is attributed to a strength difference.

The development and escape of the mushroom-type structures is analysed in more detail with 2D HiRes-PV experiments. For $Re_D = 75$ and $Ri_D = 1.3$ the process of a growing secondary structure is analysed by considering the vorticity contours of the out-of-plane component ω_z at two different time stages. At the first stage (Fig. 8:left) the shed upper vortex structure can be observed at $(x, y) = (2.5, 0.5)$ and the lower structure at $(x, y) = (4.0, -1.0)$. These structures show some slight deformation as compared to their regular pattern for $Ri_D = 0$. The upper vortex looks like a horseshoe structure and the lower vortex like an upward stretched structure. Close to the upper vortex an area of positive vorticity is found. About one and a half periods later (Fig. 8:right) this area has grown in strength. Simultaneously, the surrounding negative structure stretches and an upward moving vorticity strand is formed, which becomes separated from the primary structure. This separated blob of negative vorticity forms a dipole like structure with the further developed area of positive vorticity. This dipole structure accelerates in positive y-direction and eventually leaves the interrogation area.

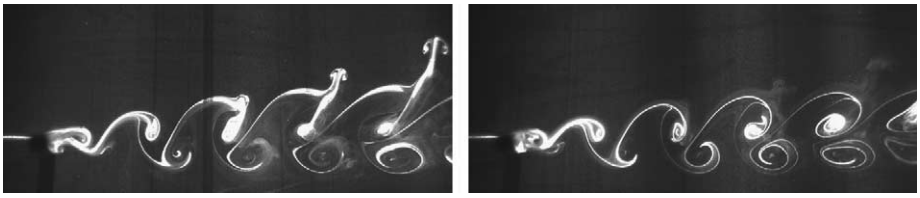

Fig. 7. Visualisation of the flow behind a heated cylinder: side-view. $Re_D = 116$, $Ri_D = 1$, 'in-plume' visualisation (left) and 'between-plume' visualisation (right) (from Rindt et al., 2001).

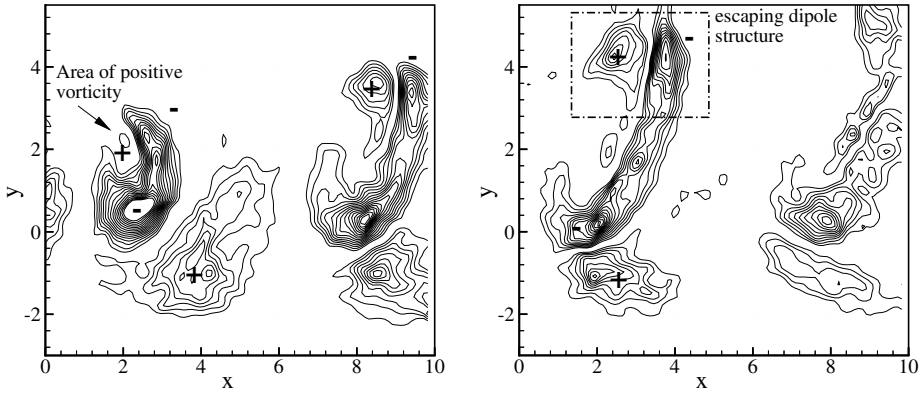

Fig. 8. Measured iso-vorticity contours of ω_z at two time levels (from Kieft et al., 2000a). The cylinder position is $x_c = -9.8$ (left) and $x_c = -19.5$ (right).

From experiments it appeared that the initial process of a growing secondary structure, as discussed above, is more or less 2D. In order to analyse the development from a 2D to a 3D flow, this process is also analysed numerically using the 2D code. Both the numerical and experimental results show a similar evolution for the first stages. For later stages, a difference appears between the experimental and the 2D numerical results. This allows to conclude that initially the development of the secondary structure is a more or less 2D process but the escaping process (formation of a dipole structure and acceleration) is a 3D phenomenon.

5.2. Near-wake behaviour

The occurrence of mushroom-type structures emerging from the upper vortex row was investigated in more detail with tin-visualisation experiments (Rindt et al., 2001). The tinned anode plate was positioned in such a way that the visualisation sheet moved through the upper boundary layer of the cylinder. To get a first impression of the occurring structures, the whole volume behind the heated cylinder was illuminated. The camera was positioned above the cylinder (with some angle with respect to the gravity vector). The slight bending of the structures in span-wise direction, as observed in Fig. 9:left and middle, is caused by the lens distortion. The experiments show that the shed vortex rolls are two-dimensional for $Ri_D < 0.3$ (see Fig. 9:left for $Ri_D = 0.15$). For $Ri_D > 0.3$ 3D structures are visible in the vortex rolls as well as in the braids. These structures initially do not result in large deformations. In Fig. 9: middle for $Ri_D = 1$, some distance downstream of the cylinder the formation of thermal plumes can be seen.

The visualisations for different Ri_D at $Re_D = 102$ and 75 showed the same behaviour as for $Re_D = 117$ although the Richardson numbers at which the phenomena start and the quantitative measures may be different. From the visualisations it appears that the flow is 3D far before the thermal plumes escape from the vortices. The three-dimensionality even seems to go back completely to the cylinder, which can be seen in Fig. 9: middle. From this figure it can be concluded that the spanwise positions, at which further downstream the thermal plumes are formed, are already determined at the rear end of the cylinder.

In Fig. 9:right a snapshot is given of the three-dimensional structure at the rear end of the cylinder for $Re_D = 117$ and $Ri_D = 1$. The 'vortical structure' manifests itself as two counter-rotating vortices. From the visualisations it followed that at the moment the upper vortices are shed, fluid is convected towards the spanwise positions at which further downstream the plumes are formed. These convection flows may lead to spanwise temperature differences in the vortex rolls. The occurring counter rotating vortices seem to be highly linked to the observed deformations of the vortex rolls and vortex braids. The spanwise position of the midplanes of these twin-vortices exactly coincides with the spanwise position of the thermal plumes further downstream. From experiments in which the Richardson number was varied, it is concluded that the above discussed 3D transition sets in at $Ri_D \approx 0.3$. The spanwise distance of the vortical structures is hardly influenced by the Richardson number and remains rather constant around a value of 2D.

6. Conclusions

The results show that due to the heat added by the cylinder, the vortices in the upper and lower vortex row

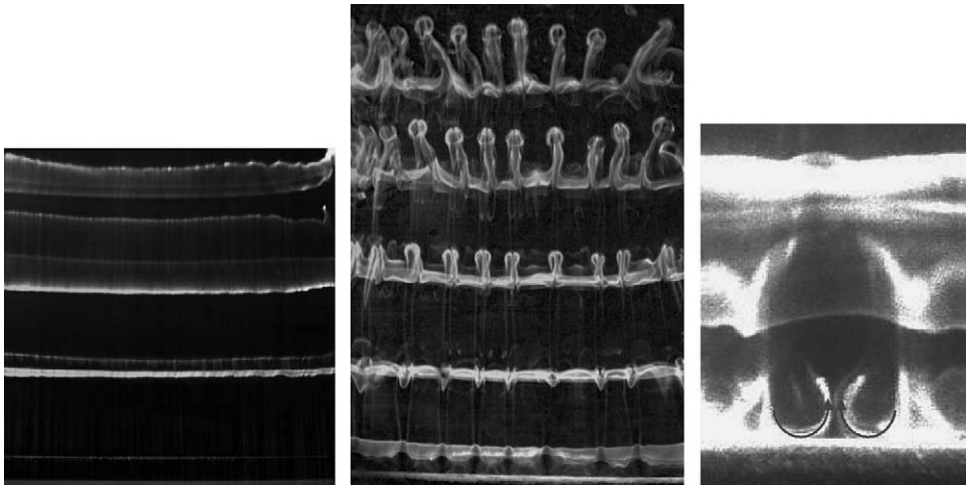

Fig. 9. Overview pictures of the vortex shedding for $Re_D = 117$ and $Ri_D = 0.15$ (left) and $Ri_D = 1.0$ (middle) (from Rindt et al., 2001) and vortical structure at the rear end of the cylinder for $Re_D = 117$ and $Ri_D = 1$ (right). The flow is from bottom to top, the cylinder is positioned at the bottom.

acquire different strengths (in absolute sense). This strength difference increases for increasing Ri_D and is already present just after the vortex structures are shed. As a result, the shed vortices are seen to move slightly downwards. At first sight, this is a rather unexpected behaviour, considering the upward action of the buoyancy force. By using a point-vortex model it can be shown that the strength difference is indeed responsible for the observed negative deflection (Kieft et al., 1998, 1999a). The point-vortex model predicts a continuously increasing downward shift of the vortices. This is in contrast to the experimental and numerical results, which show a maximum downward deflection for $Ri_D = 0.5$. For higher values of Ri_D the thermally induced buoyancy force causes the vortex structures to move up again, compensating the effect of the strength difference. A second effect of the strength difference is the relative motion between the vortex structures, visible as a rotational drift of the lower vortex around its upper neighbour.

An analysis of the vorticity terms in the vicinity of the cylinder shows that for $Ri_D > 0$ slightly more positive than negative vorticity is produced and transported into the region $x > 1$. This is in contrast with the results found for the fully developed structures at $x > 8$, where the negative upper vortex structures are stronger than the lower ones (with positive vorticity). In the region $1 < x < 4$ the baroclinic vorticity production is mostly negative. Also the areas where vorticity is produced coincide with the region where a vortex structure is growing. This means that vorticity production in the region considered adds to the negative vorticity structures and causes the positive vorticity structures to become weaker.

From detailed visualisation results it appears that the wake becomes three-dimensional for $Ri_D > 0.3$. For these Richardson numbers three-dimensional 'vortical structures' are observed near the cylinder wall. Here already the spanwise positions, at which further downstream the plumes are formed, are determined. It seems that the 'vortical structures' behind the cylinder result in an extra transport of warm fluid to the upper vortices at certain spanwise positions. This may result in spanwise temperature variations in the upper vortex roll, possibly leading to baroclinic vorticity production in the streamwise direction. The net transport of heat from the lower to the upper half of the wake also seems to disturb the advection of vorticity to the lower vortices, which, in turn, results in a spanwise variation of the vortex strength.

Although 3D structures in the wake are present far before the formation of the plumes, the velocities associated with these structures are small. For this reason, a 2D consideration of the wake describes the occurring phenomena, like a negative deflection of the vortex street and the relative motion of the vortices, very well.

In future research, temperature measurements in a cross-section of the upper vortex roll will confirm (or reject) the spanwise temperature gradient hypothesis. The laser induced fluorescence technique, as presented in Seuntiëns et al. (2001), can be used for that purpose. In Fig. 10 the temperature distribution in the vortex street is given, as measured with this method, for two moments in time. The cylinder is situated at $y = x = 0$. From the results it can be concluded that the upper vortex contains more heat than the lower one, resulting in a higher temperature of the upper vortex. This is in agreement with the results of the numerical simulations in Kieft (2000).

With these proposed temperature measurements, the exact source of the 'instability' should be investigated as in Williamson (1996) for the purely forced convection case. In addition, it may be interesting to perform three-dimensional velocity measurements to examine the occurrence of the 'vortical structures' and to study the spanwise variations in vortex strengths.

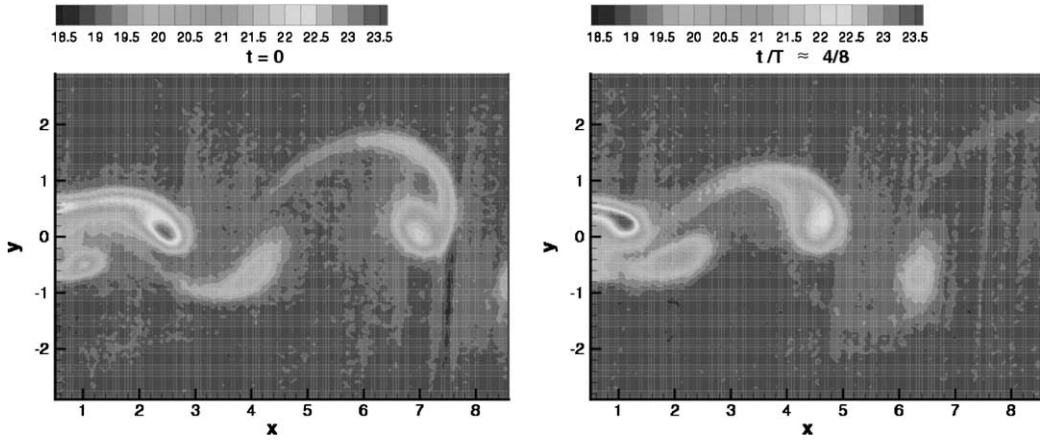

Fig. 10. Temperature distribution in the vortex street behind the cylinder (from Seuntiëns et al., 2001).

Acknowledgements

This work is part of the research programme of the Netherlands Foundation for Fundamental Research on Matters (FOM), which is financially supported by the Netherlands Organisation for Scientific Research (NWO). The authors would like to take the opportunity to thank the PhD students Rene Kieft and Maosheng Ren, the Master Students Harm Seuntiëns and Walfred Maas, and the staff member Gert van der Plas for their contributions to the results obtained.

References

Agui, C., Jimenez, J., 1987. On the performance of particle tracking. J. Fluid Mech. 185, 447–468.

Badr, H., 1984. Laminar combined convection from a horizontal cylinder-parallel and contra flow regimes. Int. J. Heat Mass Trans. 27, 15–27.

Barkley, D., Henderson, R., 1996. Three-dimensional Floquet stability analysis of the wake of a circular cylinder. J. Fluid Mech. 322, 215–241.

Bastiaans, R., van der Plas, G., Kieft, R., 2001. The performance of a new PTV algorithm applied in super-resolution PIV. Exp. Fluids 32, 346–356.

Bénard, H., 1908. Formation de centres de giration á l'arrière d'un obstacle en mouvement. Comptes Rendus Academie des Sciences 147, 970–972.

Chang, K., Sa, J., 1990. The effect of buoyancy on vortex shedding in the near wake of a circular cylinder. J. Fluid Mech. 220, 253–266.

Coolen, M., Kieft, R., Rindt, C., van Steenhoven, A., 1999. Application of 2D LIF temperature measurements in water using a Nd:YAG laser. Exp. Fluids 27, 420–426.

Cuvelier, C., Segal, A., vanSteenhoven, A., 1986. Finite Element Methods and Navier–Stokes Equations. Reidel Publ. Comp, Dordrecht, The Netherlands.

Eisenlohr, H., Eckelmann, H., 1989. Vortex splitting and its consequences on the vortex street wake of cylinders at low Reynolds numbers. Phys. Fluids 1, 189–192.

Gerrard, J., 1978. The wakes of cylindrical bluff bodies at low Reynolds number. Philos. Trans. R. Soc. London, Ser. A 5, 288–351.

Green, R., Gerrard, J., 1991. An optical interferometric study of the wake of a bluff body. J. Fluid Mech. 226, 219–242.

Green, R., Gerrard, J., 1993. Vorticity measurements in the near wake of a circular cylinder at low Reynolds numbers. J. Fluid Mech. 246, 675–691.

Hama, F., 1957. Three-dimensional vortex pattern behind a circular cylinder. J. Aeronaut. Sci. 24, 156.

Hatton, A., James, D., Swire, H., 1970. Combined forced and natural convection with low-speed air flow over horizontal cylinders. J. Fluid Mech. 42, 17–31.

Humphrey, J., Marcus, D., 1987. Some observations of a sheared Rayleigh-Taylor/Benard instability. Exp. Fluids 5, 235–239.

Karniadakis, E., Triantafyllou, G., 1992. Three-dimensional dynamics and transition to turbulence in the wake of bluff bodies. J. Fluid Mech. 238, 1–30.

Kieft, R., Rindt, C., van Steenhoven, A., 1998. The influence of buoyancy on the behavior of the vortex structures in a cylinder wake. In: Lee, J.S. (Ed.), Proceedings 11th International Heat Transfer Conference, vol. 3, pp. 219–224.

Kieft, R., Rindt, C., van Steenhoven, A., 1999a. The wake behaviour behind a heated horizontal cylinder. Exp. Therm. Fluid. Sci. 19, 183–193.

Kieft, R., Rindt, C., van Steenhoven, A., 1999b. Destabilising effects of heat on coherent structures. In: Banerjee S., Eaton, J. (Eds.), Proceedings Int. Symp. on Turbulence and Shear Flow Phenomena, pp. 1027–1032.

Kieft, R., 2000. Mixed convection behind a heated cylinder. PhD thesis, Eindhoven University of Technology, The Netherlands.

Kieft, R., Rindt, C., van Steenhoven, A., 2000a. 3D-transition of low Reynolds number flow around a heated cylinder. In: Hahne, E. et al. (Eds.), Proceedings 3rd European Thermal Sciences Conference, Edizioni ETS, Pisa, pp. 659–664.

Kieft, R., Rindt, C., van Steenhoven, A., 2000b. The influence of baroclinic vorticity production on the stability of the wake behind a heated cylinder. In: Nagano, Y. et al. (Eds.), Proceeding 3rd Int. Symp. on Turbulence, Heat and Mass Transfer, pp. 315–322.

Kieft, R., Rindt, C., van Steenhoven, A., 2002a. Heat induced transition of a stable vortex street. Int. J. Heat Mass Transfer 45, 2739–2753.

Kieft, R., Schreel, K., Plas, G., Rindt, C., 2002b. The application of a 3D-PTV algorithm to a mixed convection flow. Exp. Fluids 33, 603–611.

Kieft, R., Rindt, C., van Steenhoven, A., van Heijst, G., in press. On the wake structure behind a heated horizontal cylinder in cross-flow. J. Fluid Mech.

Lecordier, J., Hamma, L., Paranthoën, P., 1991. The control of vortex shedding behind heated circular cylinders at low Reynolds numbers. Exp. Fluids 10, 224–229.

Lecordier, J., Browne, L., Le Masson, S., Dumouchel, F., Paranthoën, P., 2000. Control of vortex shedding by thermal effect at low Reynolds numbers. Exp. Thermal Fluid Sci. 21, 227–237.

Maas, W., Rindt, C., van Steenhoven, A., in press. The influence of heat on the 3D-transition of the von Kármán vortex street. Int. J. Heat Mass Transfer.

Mi, J., Antonia, R., 1994. Temperature distribution within vortices in the wake of a cylinder. Int. J. Heat Mass Transfer 37, 1048–1050.

Michaux-Leblond, N., Bélorgey, M., 1997. Near-wake behavior of a heated circular cylinder: viscosity–buoyancy duality. Exp. Therm. Fluid Sci. 15, 91–100.

Minev, P., van de Vosse, F., Timmermans, L., van Steenhoven, A., 1995. A second order splitting algorithm for thermally-driven flow problems. Int. J. Numer. Meth. Heat Fluid Flow 6, 51–60.

Mittal, R., Balachandar, S., 1996. Direct numerical simulation of flow past elliptic cylinders. J. Comput. Phys. 124, 351–367.

Noto, K., Ishidea, H., Matsumoto, R., 1985. A break-down of the von Kármán vortex street due to the natural convection. In: Flow Visualization, vol. 3. Springer, Berlin, pp. 348–354.

Noto, K., 1991. Computational investigation on wake behavior with buoyancy from a heated elliptic cylinder: Effect of mainstream attack angle. Thirty-ninth Japanese National Congress of Applied Mechanics, pp. 293–303.

Noto, K., Matsumoto, R., 1987. Numerical simulation on the development of the Karman vortex street due to the negatively buoyant force. In: Fifth Conference on Numerical Methods in Laminar Flow. Pineridge Press, Swansea, pp. 796–809.

Rindt, C., Maas, W., van Steenhoven, A., 2001. 3D-transition of the wake flow behind a heated cylinder. In: Lindborg, E. et al. (Eds.), Second Int. Symp. on Turbulence and Shear Flow Phenomena, Stockholm, Sweden.

Roshko, A., 1954. On the development of turbulent wakes from vortex streets. NACA Rep. 1191.

Seuntiëns, H., Kieft, R., Rindt, C., van Steenhoven, A., 2001. 2D temperature measurements in the wake of a heated cylinder using LIF. Exp. Fluids 31, 588–595.

Singh, S., Biswas, G., Mukhopadhyay, A., 1988. Effect of thermal buoyancy on the flow through a vertical channel with a built-in circular cylinder. Numer. Heat Transfer: Part A 34, 769–789.

Slaouti, A., Gerrard, J., 1980. An experimental investigation of the end effects on the wake of a cylinder towed through water at low Reynolds number. J. Fluid Mech. 112, 297–314.

Timmermans, L., Minev, P., van de Vosse, F., 1996. An approximate projection scheme for incompressible flow using spectral elements. Int. J. Numer. Meth. Fluids 22, 673–688.

von Kármán, T., Rubach, H., 1912. Über den Mechanismus des Flüssigkeits- und Luftwiderstandes. Physikalische Zeitschrift 13, 49–59.

Wang, A., Trávníček, Z., Chia, K., 2000. On the relationship of effective Reynolds number and Strouhal number for the laminar vortex shedding of a heated circular cylinder. Phys. Fluids 12, i1401–1410.

Williamson, C., 1988. The existence of two stages in the transition to three-dimensionality of a cylinder wake. Phys. Fluids 31, 3165.

Williamson, C., 1989. Oblique and parallel modes of vortex shedding in the wake of a circular cylinder at low Reynolds numbers. J. Fluid Mech. 206, 579–627.

Williamson, C., 1992. The natural and forced formation of spot-like 'vortex dislocations' in the transition of a wake. J. Fluid Mech. 243, 393–441.

Williamson, C., 1996. Three-dimensional wake transition. J. Fluid Mech. 328, 345–407.

Wu, J., Sheridan, J., Welsh, M., Hourigan, K., 1996. Three-dimensional vortex structures in a cylinder wake. J. Fluid Mech. 312, 201–222.

Zhang, H., Fey, U., Noack, B., König, M., Eckelmann, H., 1995. On the transition of the cylinder wake. Phys. Fluids 7, 779–794.